Supporting Information

Schütz et al. 10.1073/pnas.1707974114

Combined Fits of Chemical Shift and CPMG Data

As described in the main text, we have analyzed both chemical shift and CPMG data simultaneously, focusing on R95G ND1Lp97-ADP that has significantly larger dispersion profiles than the other disease mutants. Our goal is to use a simple model that explicitly takes into account the up/down equilibrium (see below) in a description of the NTD dynamics. One possible scheme is

$$D \underset{k_{UD}}{\overset{k_{DU}}{\rightleftarrows}} U \underset{k_{CU}}{\overset{k_{UC}}{\rightleftarrows}} C, \qquad \text{[S1]}$$

where D and U denote the NTD down (WT p97-ADP) and up (WT p97-ATP) states (Fig. 1*A*), respectively, and C is an additional state. States D and U are in fast exchange, as evidenced by the linear titration of chemical shifts as a function of disease mutant severity (Fig. 1*B*) (13) and a lower limit of the D–U exchange rate (2,000 s^{-1}) could be established from the chemical shifts of pure up and pure down states that were measured in spectra of WT p97 (see main text). The combined analysis of dispersion and chemical shift data allows us to refine this estimate. Consistent with the rapid exchange between D and U (see below), we could fit our data equally well to a model where the positions of D and U are reversed in Eq. **S1** above, and, of course, to a more complex triangular model.

To link states D and U to the pure down and pure up NTD conformations, respectively, $\Delta\varpi_{DU} = \varpi_U - \varpi_D$ values (ppm) were equated to chemical shift differences observed experimentally in spectra of p97-ATP (U) and p97-ADP (D) based on five methyl groups (Ile189 δ_1, Leu213 δ_1, Leu229 δ_1, Met388 ε_1, and Met442 ε_1), and the chemical shift values of carbons of these methyls were included in the fits (see text and below). These five methyl groups were chosen based on the following criteria: (*i*) they have the largest ^{13}C chemical shift differences between the p97-ATP and p97-ADP states; (*ii*) they are not close in space to position 95; and (*iii*) they are not proximal to the terminal phosphate of ATP, so that although they are sensitive reporters of the NTD up/down equilibrium, they are not influenced directly by bound nucleotide.

Twenty-two dispersion profiles were identified as nonflat [$\Delta R_{2,eff} > 1.5\ s^{-1}$, where $\Delta R_{2,eff} = R_{2,eff}(\nu_{CPMG} = 50\ \text{Hz}) - R_{2,eff}(\nu_{CPMG} = 2{,}000\ \text{Hz})$] and used in the three-state analysis. Methyl-TROSY–based profiles were fit as described previously (24) and exchange parameters extracted by minimization of a χ^2 function (Eq. **S2**) that also included a term to enforce the ^{13}C chemical shift values of the five residues indicated above,

$$\chi^2 = \sum_{\nu_{CPMG}} \sum_{j} \left(\frac{I_j^{\text{exp}}(\nu_{CPMG}) - I_j^{fit}(\nu_{CPMG})}{\sigma_{CPMG}} \right)^2 + \sum_{k} \left(\frac{\omega_k^{\text{exp}} - \omega_k^{fit}}{\sigma_\omega} \right)^2. \qquad \text{[S2]}$$

In Eq. **S2**, the first and second terms are fitting functions for dispersion profiles and chemical shifts, respectively; j and k denote the 22 (j) dispersion profiles and the five (k) residues that are included in the fit; $I_j(\nu_{CPMG})$ is the intensity of a peak in the dispersion data set recorded with a CPMG frequency of ν_{CPMG}; ω_k is the ^{13}C shift (rad/s) of residue k measured in ^{13}C-^{1}H HMQC spectra of R95G ND1Lp97-ADP; and σ_{CPMG}, σ_ω are errors in $I_j^{\text{exp}}(\nu_{CPMG})$, as evaluated from repeat measurements, and in ω_k (6 Hz = 2π*6 rad/s), respectively, based on measured positions of cross-peaks in separate samples of R95G ND1Lp97-ADP.

Values of ω_k^{fit} were obtained by evaluating the time evolution of magnetization using the following set of equations:

$$\frac{d}{dt}\begin{pmatrix} D_x \\ D_y \\ U_x \\ U_y \\ C_x \\ C_y \end{pmatrix} = \begin{bmatrix} -k_{DU} & -\omega_D & k_{UD} & 0 & 0 & 0 \\ \omega_D & -k_{DU} & 0 & k_{UD} & 0 & 0 \\ k_{DU} & 0 & -k_{UD}-k_{UC} & -\omega_U & k_{CU} & 0 \\ 0 & k_{DU} & \omega_U & -k_{UD}-k_{UC} & 0 & k_{CU} \\ 0 & 0 & k_{UC} & 0 & -k_{CU} & -\omega_C \\ 0 & 0 & 0 & k_{UC} & \omega_C & -k_{CU} \end{bmatrix} \begin{pmatrix} D_x \\ D_y \\ U_x \\ U_y \\ C_x \\ C_y \end{pmatrix}, \qquad \text{[S3]}$$

where A_j denotes the $j \in (x, y, z)$ component of spin $A \in (D,U,C)$ and ω_A is the ^{13}C resonance frequency of spin A with starting magnetization values of $[p_D, 0, p_U, 0, p_C, 0]$, where p_A is the fractional population of state A. Values of each of the six elements ($D_x \ldots C_y$) were evaluated over an interval of 70 ms, starting from 0, to produce numerical values for the total magnetization, $M^+(t) = M_x(t) + iM_y(t)$, ($i = \sqrt{-1}$). $M^+(t)$ was apodized and then Fourier transformed; the position of the peak in the simulated spectrum was fitted to estimate ω_k^{fit}. The parameters that were fixed/fit in our analysis (using the program ChemEx and a new fitting module that is available upon request) are summarized below:

Parameter name	Description	Floating/fixed
ω_D	Chemical shifts of down state	Fixed for five selected residues (^{13}C only) and used in Eq. **S3**
$\Delta\omega_{UD} = \omega_D - \omega_U$	Difference in chemical shifts between up and down states	Fixed for five selected residues (^{13}C and ^{1}H) and floating for others
$\Delta\omega_{CD} = \omega_D - \omega_C$	Difference in chemical shifts between states C and D	Floating
$R_{MQ,D}$, $R_{MQ,U}$, $R_{MQ,C}$	Multiple quantum (MQ) relaxation rates for states D, U, C	Floating, but assumed the same for a given methyl
$k_{ex,DU}$, $k_{ex,UC}$, p_U, p_C	Exchange rates and populations	Floating global parameters

It is worth noting that ^{13}C-^{1}H HMQC dispersion profiles are sensitive to differences in both methyl ^{1}H and ^{13}C chemical shifts (24) and both of these differences are either fit or fixed as described above. Fig. 2*B* presents 1D χ^2_{red} surfaces for $k_{ex,DU}$ and $k_{ex,UC}$ from which it is clear that $k_{ex,DU} > 15{,}000\ s^{-1}$ and $1{,}500\ s^{-1} \leq k_{ex,UC} < 4{,}000\ s^{-1}$. Values of $p_U = 0.41$ and $p_C = 0.09$ are obtained from fits.

As described in the main text, dispersion profiles could be well fit to a two-state model, $G \rightleftarrows E$; however, the extracted chemical shift differences, $\Delta\varpi_{GE}$, did not correspond to $\Delta\varpi_{DU}$. Because the interconversion between states *D* and *U* is fast (>15,000 s^{-1}; see above), it is possible to derive a simple relation between $\Delta\varpi_{GE}$ and the $\Delta\varpi$ values that are extracted from the three-state fit by noting that the up/down exchange averaged positions of resonances in spectra are given by

$$\varpi_{averaged} = \varpi_D + \frac{p_U}{p_U + p_D}\Delta\varpi_{DU} \qquad \textbf{[S4]}$$

and thus the fitted shift difference assuming a two-state model, $\Delta\varpi_{GE}$, can be expressed as

$$\begin{aligned}\Delta\varpi_{GE} &= \varpi_C - \varpi_{averaged} \\ &= -\Delta\varpi_{CD} + \frac{p_U}{p_U + p_D}\Delta\varpi_{UD}.\end{aligned} \qquad \textbf{[S5]}$$

We have verified that Eq. **S5** holds. An advantage of the three-state fits is that it becomes possible to quantify the lower bound for the *D*–*U* exchange rate.

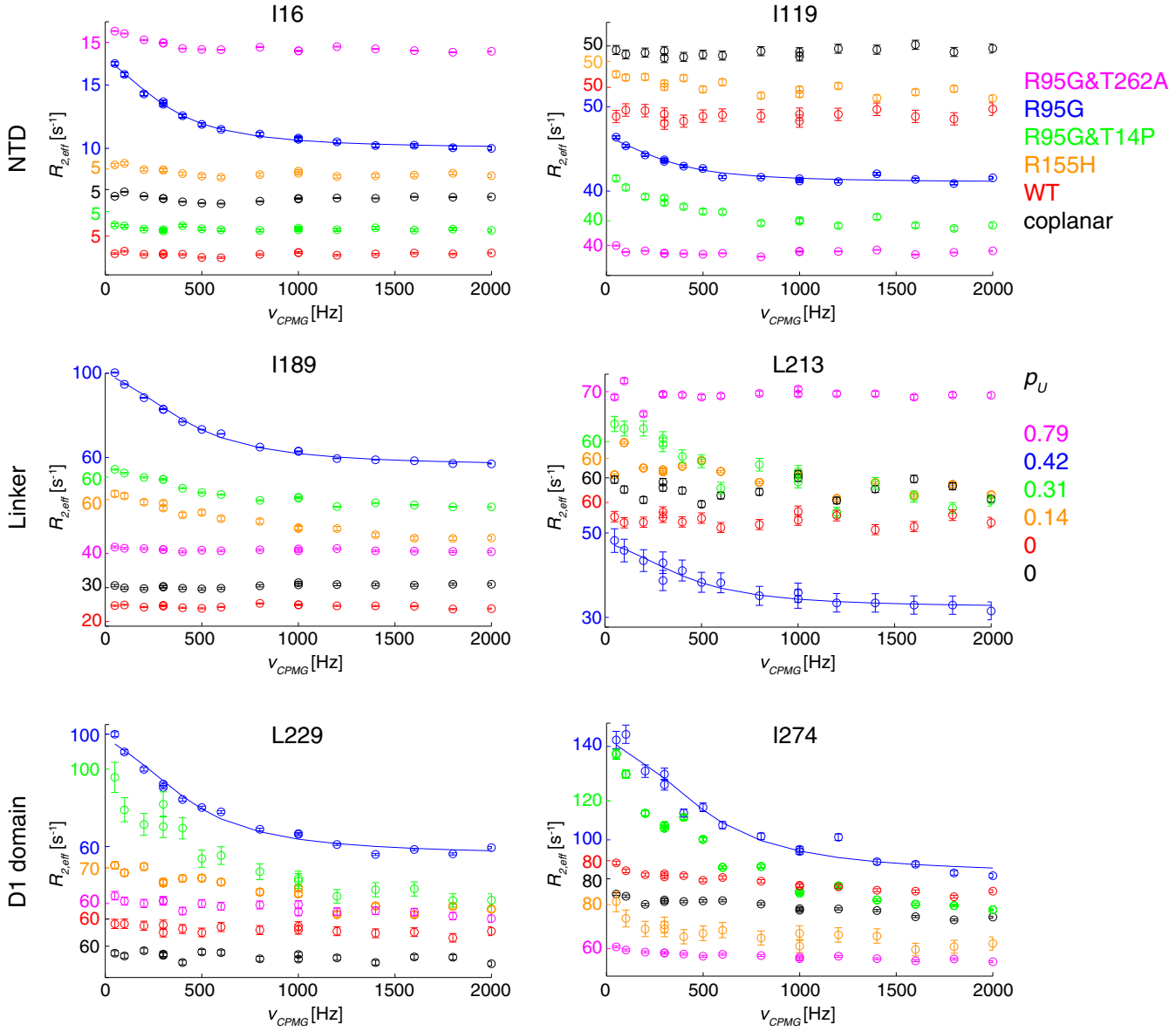

Fig. S1. ^{13}C-^{1}H multiple-quantum relaxation dispersion profiles from experiments recorded on WT ND1Lp97-ADP (red) and the following mutants: R95G&T262A (magenta), R95G (blue), R95G&T14P (green), R155H (orange), and R95G-coplanar (black). All p97 constructs were in the ADP loaded state. Selected residues are located in the NTD (I16, I119), in the NTD–D1 linker (I189, L213), and in the D1 domain (L229, I274). Notably, dispersion profiles are largest for R95G ND1Lp97-ADP and decrease as p_U becomes either larger or smaller than ~0.5. Nonflat dispersion profiles were obtained for a small number of residues in R155H ND1Lp97-ADP (6) and for 15 residues in T14P,R95G ND1Lp97-ADP where the interface between the N terminus of the NTD and the D1 domain of an adjacent protomer has been modified by removal of the N-terminal NTD helix (T14P; see text). For all other variants considered, profiles were essentially flat. All residue-specific dispersion curves from different mutants have been offset slightly for ease of visualization; *y* axis values are color-coded differently for each mutant, as indicated. Note the different plateau values for dispersion profiles (taking into account the different offsets), which likely indicates a diversity of fast timescale dynamics (faster than ν_{CPMG}) both as a function of position within a given p97 variant and between variants. A case in point is provided by I16, located in a flexible loop region in the down state that undergoes a secondary structure change to a helix that folds back onto the D1 hexamer, in the up state. Plateau values of ≈5 s^{-1} are obtained for profiles from this residue when the NTDs are in the down (WT, disulfide linked) or predominantly down (R155H) conformations, or when the helix cannot form due to mutation (R95G&T14P), yet increase to 10–15 s^{-1} when the NTDs are partially up (R95G, R95G&T262A). Trends for other residues can sometimes be more difficult to rationalize, but it is worth noting that, as discussed in the text, the position of the plateau is influenced not only by dynamics but also by the magnitude (and sign) of ^{1}H $\Delta\varpi$ in multiple quantum-based CPMG experiments (24).

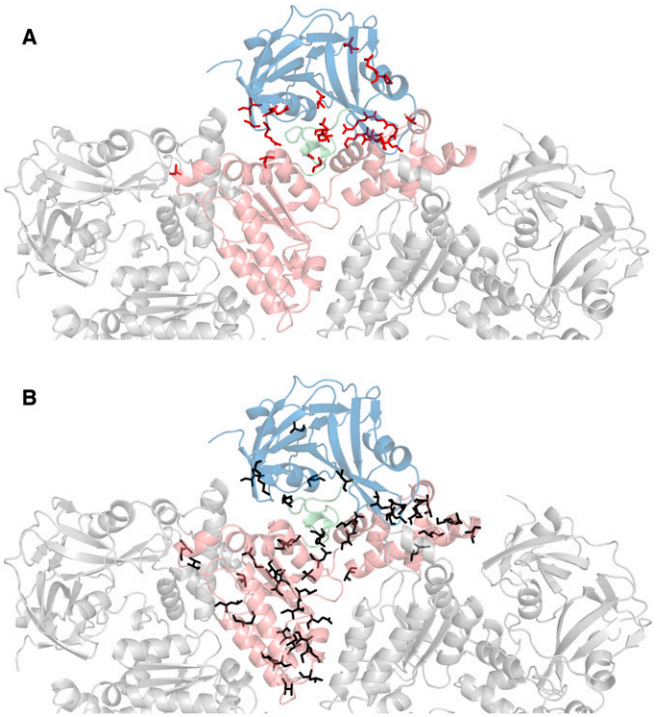

Fig. S2. Location of disease-associated mutations (*A*) (12) and predominantly hydrophobic substitutions that have been tested (*B*) in ND1Lp97. Top view of a half-hexamer of ND1Lp97-ADP in cartoon representation with the central protomer color-coded by domain (NTD-linker-D1 in blue, green, red). (*A*) The 22 residues in ND1Lp97 that are mutated in disease patients (12) are shown in red (sticks) on the structure of the ADP state [PDB ID code 1E32 (33)]. (*B*) Black sticks denote the positions of 56 point mutations that do not shift the NTD up/down equilibrium in p97-ADP.

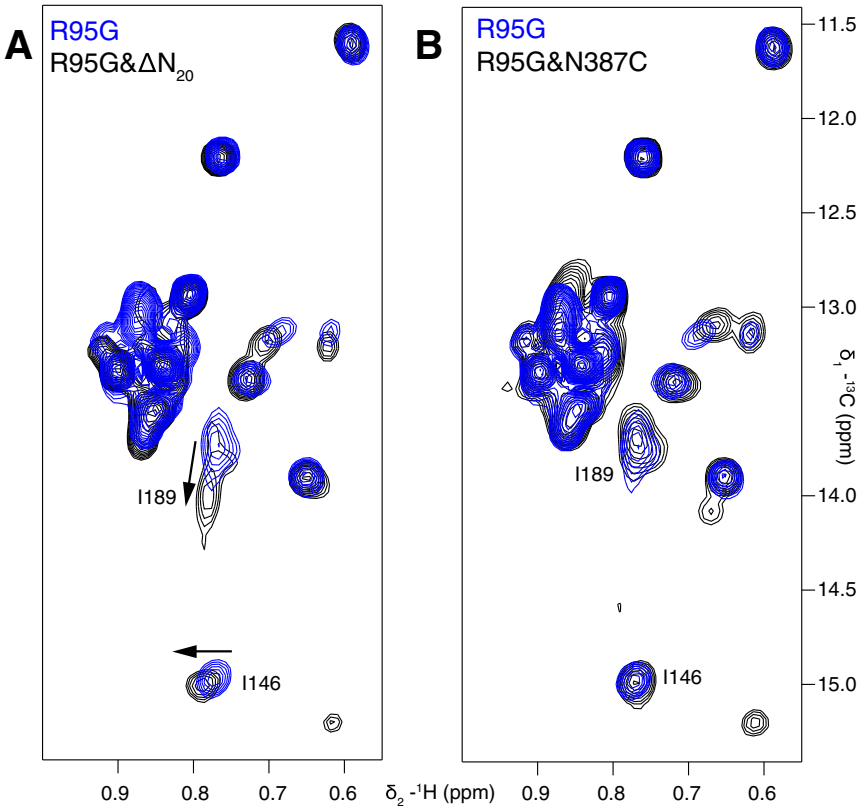

Fig. S3. Effect of mutations on the NTD equilibrium in R95G ND1Lp97-ADP. Superposition of the isoleucine region from ^{13}C-^{1}H HMQC spectra (18.8T, 50 °C) focusing on I146δ_1 and I189δ_1 cross-peaks that report on the NTD up/down equilibrium. (*A*) The ΔN_{20} deletion in the R95G context (black contours) partially restores the equilibrium to the down position (blue to black). (*B*) Position 95 is distal from the N387C mutation, and thus, unlike the case for R155C ND1Lp97-ADP (see text), the N-to-C substitution at position 387 has no effect on the NTD equilibrium in R95G ND1Lp97-ADP (as evidenced by the superposition of blue and black peaks).

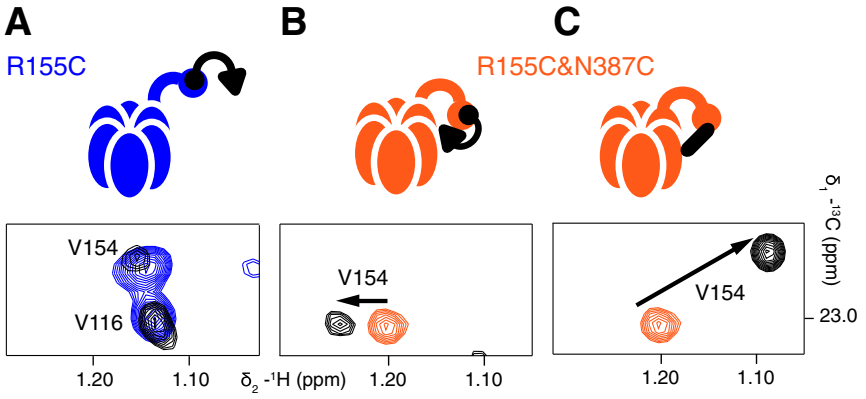

Fig. S4. V154 is a proxy for disulfide bond formation between proximal C155 and C387 residues in R155C,N387C ND1Lp97-ADP. Selected regions of ^{13}C-^{1}H HMQC spectra are shown highlighting the resonance position of the δ_1 methyl group of V154. (*A*) R155C ND1Lp97-ADP (blue, no UBXD1-N; black, threefold excess UBXD1-N over p97 protomers). As indicated schematically above the spectrum, binding of UBXD1-N to the NTD occurs via the VIM domain (black circle) but the H1/H2 motif (black triangle) is not able to interact, and there is no change in the peak position of V154. (*B*) In the R155C,N387C ND1Lp97-ADP variant, the up/down equilibrium is restored to the WT situation and WT two-pronged binding of UBXD1-N is observed (see main text and schematic). The position of V154 shifts slightly to reflect this, as indicated by the arrow. Sample is prepared with 5 mM TCEP. (*C*) A large chemical shift change is observed for V154 δ_1 that reflects formation of the 155–387 disulfide in R155C,N387C ND1Lp97-ADP under oxidizing conditions (orange, 5 mM TCEP; black, oxidizing conditions). UBXD1-N is not added in this case.

Table S1. Point mutations that do not perturb the up/down NTD equilibrium in ND1Lp97-ADP

Mutation at	Mutated to	CSP*	RD†	Other observations	Mutation at	Mutation to	CSP*	RD†
L17	I			Located in N-terminal helix that is formed in the ATP state only	V320	I		
I27	V	x		Associated with disease (38) but also found in healthy control patients (12)	I324	V		
I32	V		x		V325	I		
K63	A			Affects salt bridge formation in ATP state	M332	L		
	E							
V71	I				L335	M		
V123	I	x			V341	I		
I126	L				M344	I		x
M158	L	x		Location of disease mutation M158V	I353	V		x
I189	V	x	x	Located at the beginning of linker helix	V367	I		
E194	P			Located in the middle of linker helix; affects helix formation in ATP state	I369	V		
V201	I		x	Located at the end of linker helix	L378	M		
I206	V			Location of disease mutation I206F	I380	V		
L213	M	x	x		I383	V		
M219	L		x		M388	L	x	x
I233	L				V407	T		
V235	I				L420	M		
L253	I				I423	V		
V258	I				M427	L		x
L268	M				L429	M		
I269	V				L432	I		
I274	V	x	x		M442	L		x
M275	L				L445	M	x	
L278	M				V447	I		
I300	V				L464	M		
E305	Q			Walker B position	V468	I		
I309	V				V471	L		

*For each residue, it is noted whether the δ_1 (Ile), γ_1 (Val), or δ_1 (Leu) methyl peak position is sensitive to the NTD up/down equilibrium [x, combined ^{13}C and ^{1}H chemical shift differences between ND1Lp97-ADP and R95G mutant exceeds 0.25 ppm, $\sqrt{(0.25\Delta\varpi_C)^2 + (\Delta\varpi_H)^2} > 0.25$ ppm, where $\Delta\varpi$ is in ppm].
†The x indicates that $\Delta R_{2,eff} > 1.5\ s^{-1}$, where $\Delta R_{2,eff} = R_{2,eff}$ (ν_{CPMG} = 50 Hz) − $R_{2,eff}$ (ν_{CPMG} = 2,000 Hz) in relaxation dispersion profiles recorded on R95G ND1Lp97-ADP.

Table S2. Point mutations that perturb the up/down equilibrium in ND1Lp97-ADP

Mutation*	Mutation to	Class†	Background**	p_U (from background)‡	Observations
ΔN_{20}	Deletion of residues 1–20	A	R95G ND1Lp97-ADP	0.31 (0.42)	
T14	P	A	R95G ND1Lp97-ADP	0.31 (0.42)	I16 uncoupled from CPMG dynamics
A15	P	A	R95G ND1Lp97-ADP	0.31 (0.42)	I16 uncoupled from CPMG dynamics
K63	A,E	A	WT ND1Lp97-ADP	0 (0)	
	A	A	R95G ND1Lp97-ADP	0.33 (0.42)	
R95	G	D	WT ND1Lp97-ADP	0.42 (0)	
R155	H	D	WT ND1Lp97-ADP	0.14 (0)	
	C	D	WT ND1Lp97-ADP	0.45 (0)	
	P	D	WT ND1Lp97-ADP	0.51 (0)	
R191	Q	D	WT ND1Lp97-ADP	0.39 (0)	
E194	P	A	WT ND1Lp97-ADP	0 (0)	NTD/D1 linker helix broken but NTD equilibrium
	P	A	R95G ND1Lp97-ADP	0.42 (0.42)	not shifted as evident from other residues
	P	A	WT ND1Lp97-ATPgS	1.0 (1.0)	(e.g., I146, M388, M442)
L198	W	D	WT ND1Lp97-ADP	0.27 (0)	
A232	E	D	WT ND1Lp97-ADP	0.18 (0)	
N387	C	A	WT ND1Lp97-ADP	0 (0)	
	C	A	R95G ND1Lp97-ADP	0.42 (0.42)	
	C	A	R155C ND1Lp97-ADP	0.06 (0.45)	Under reducing conditions
	C	A	R155C ND1Lp97-ADP	0.00 (0.45)	Under oxidizing condition, cross-linked
	C	A	R155P ND1Lp97-ADP	0.31 (0.51)	
	H	D	WT ND1Lp97-ADP	0.14	

*Data from our previous study (13) and the present work were compiled.
**p_U values for the construct listed under Background are given in parentheses.
†Mutations are classified as artificial (A) or naturally occurring, disease causing (D).
‡The population of the up state is given, p_U, as determined from the position of the I189 correlation (except for E194P mutants; see text).